Modeling of the cardiac sympathetic nervous system and the contribution of epicardium-derived cells

Ge, Y.

PART III

CARDIAC SYMPATHETIC NERVOUS SYSTEM REMODELING AFTER CARDIAC DAMAGE

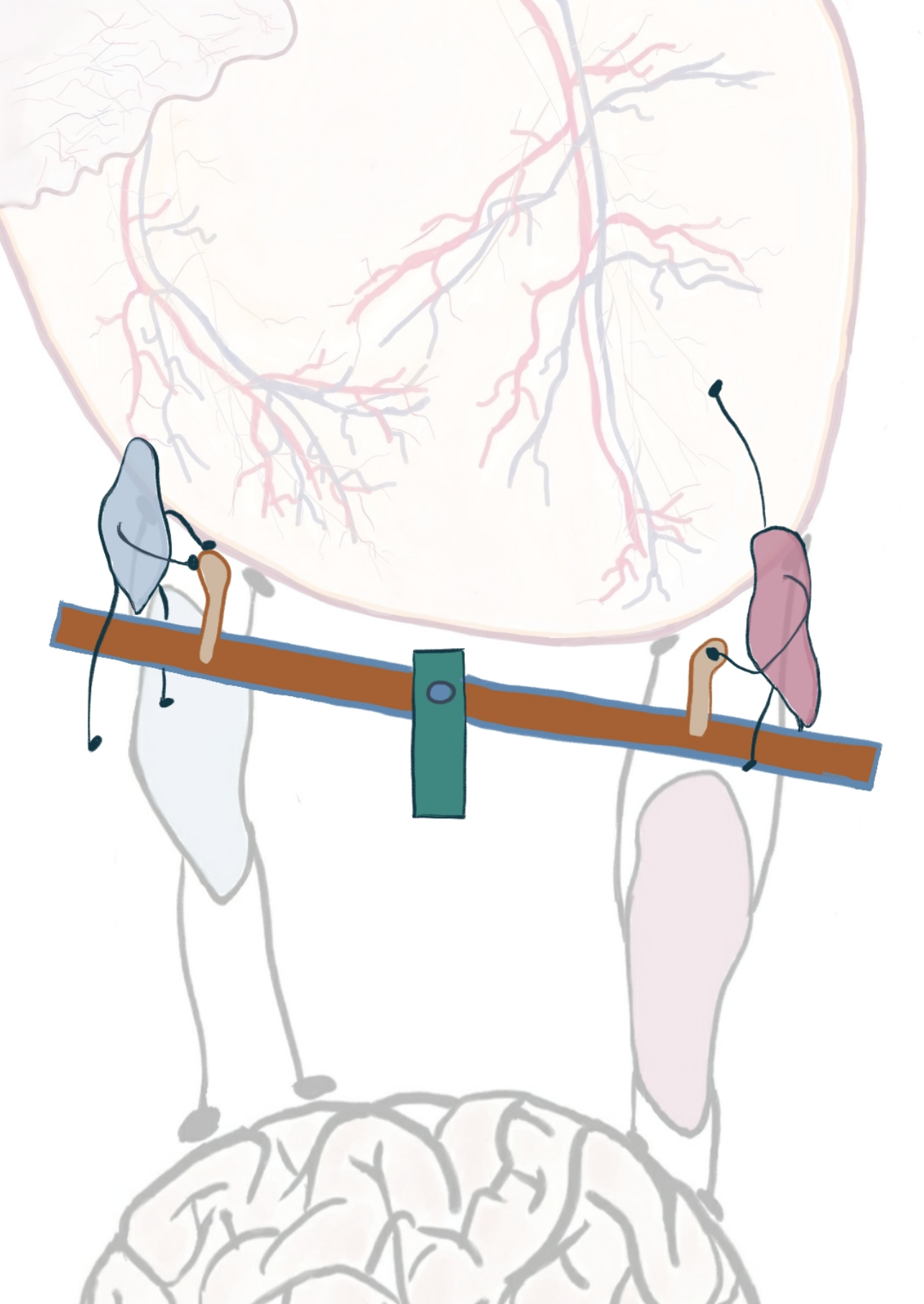

5

ACUTE MYOCARDIAL INFARCTION INDUCES NEURONAL REMODELING IN MURINE SUPERIOR CERVICAL GANGLIA

Yang Ge[1,2], Lieke van Roon[1,2], Janine M. van Gils[4], Conny J Munsteren[1] , Anke M. Smits[3], Marie-José T.H. Goumans[3], Marco C. DeRuiter[1], Monique R.M. Jongbloed[1,2]

1. Department of Anatomy & Embryology, Leiden University Medical Center, Einthovenweg 20, 2333 ZC Leiden, The Netherlands;

2. Department of Cardiology, Leiden University Medical Center, Albinusdreef 2, 2333 ZC Leiden, The Netherlands;

3. Department of Cell and Chemical Biology, Leiden University Medical Center, Einthovenweg 20, 2333 ZC Leiden, The Netherlands

4. Department of Nephrology, Leiden University Medical Center, Albinusdreef 2, 2333 ZC Leiden, The Netherlands;

Under revision *Frontiers in cardiovascular medicine*

ABSTRACT

A role for cardiac sympathetic hyperinnervation in arrhythmogenesis after myocardial infarction (MI) has increasingly been recognized. In humans and mice, the heart receives cervical as well as thoracic sympathetic contributions. In mice, superior cervical ganglia (SCG) have been shown to contribute significantly to myocardial sympathetic innervation of the left ventricular anterior wall. Of interest, the SCG is situated adjacent to the carotid body (CB), a small organ involved in oxygen and metabolic sensing. We investigated the remodeling of murine SCG, as well as the adjacent CB, over time after MI. Murine SCG were isolated from control mice, as well as 24 hours, 3 days, 7 days and 6 weeks after MI. SCG were stained for autonomic nervous system markers (Tubb3, TH and ChAT), as well as for neurotrophic factors (BDNF and NGF) and their receptors. Quantification of the staining-intensity as well as the neuronal size was performed in the entire SCG and in the adjacent CB. Our results show that ChAT and TH are co-expressed in SCG neuronal cells in control ganglia. After MI, neuronal remodeling occurs, with a significant increase in size of ganglionic cells and a decreased intensity of ChAT expression. This SCG remodeling was observed as early as 24 hours after infarction, with a peak at day 7, regressing within 6 weeks post-MI to basal levels. Of note, the most robust neuronal remodeling was observed at the region adjacent to the CB. An increase of neurotrophic factors (BDNF and NGF) was observed in the CB and neuronal cells, whereas the high affinity receptors for BDNF and NGF increased in the SCG after MI. These findings were concomitant with an increase in GAP43 expression indicating axonal outgrowth in the SCG. In conclusion, overt remodeling occurs after MI in the SCG as well as in the CB, suggesting an interaction of these 2 structures that might contribute to pathological cardiac hyperinnervation.

Keywords

Myocardial infarction, murine, superior cervical ganglion, neuronal remodeling, carotid body, neurotrophic factors, TrK, GAP43

INTRODUCTION

About one third of all global deaths are attributed to cardiovascular diseases (World Health Organization, 2017). In Western countries, the incidence of sudden cardiac death (SCD) is 50-100 per 100,000 which is attributed to coronary artery disease (CAD) in 70-80% of cases, despite the development of reperfusion strategies and medical therapies (Isbister and Semsarian, 2019). SCD after myocardial infarction (MI) has been classically linked to heterogeneous conduction in the infarct border zone caused by surviving cardiomyocytes surrounding the scar area, resulting in polymorphic ventricular tachycardia (VT) based on micro-re-entry (de Bakker et al., 1993; Wit, 2017). Interestingly, in the past decades a role for the cardiac autonomic nervous system in arrhythmogenesis after MI has increasingly been recognized (Zipes and Rubart, 2006; Li and Li, 2015). The heart is innervated by the autonomic nervous system, divided in sympathetic and parasympathetic branches, regulating cardiac function. In order to maintain a regular heartbeat, a balance is needed between sympathetic and parasympathetic tone. Parasympathetic input towards the heart is provided by (branches of) the vagal nerve that synapse in parasympathetic ganglia in the epicardial layer of the heart. Preganglionic cardiac sympathetic axons synapse with postganglionic sympathetic neurons in the sympathetic chain (Wink et al., 2020). In humans, cardiac input from the sympathetic chain is provided by both cervical as well as thoracic contributions (Kawashima, 2005; Wink et al., 2020).

A myriad of studies have reported a potential association of cardiac sympathetic hyperinnervation, usually defined as an increased amount of sympathetic nerve fibres in the area of damage, with SCD after MI. To date the exact underlying mechanism of the relation between sympathetic hyperinnervation and VT after MI is still uncertain. Likely, factors secreted by the ischemic myocardium retrogradely stimulate axonal outgrowth and remodeling of sympathetic ganglia, altering electrophysiological properties, thereby increasing the risk of VT and SCD (Han et al., 2012; O'Keeffe et al., 2016; Irie et al., 2017). Recent data shows an upregulation of nerve growth factor (NGF) in the ischemic zone after MI, that supports this concept (Ge et al., 2020).

Although several studies have shown sympathetic hyperinnervation as well as neuronal remodeling post-MI, the exact timeline of this phenomenon is less clear. In several species, neuronal remodeling has been described to occur 1 to 8 weeks after MI, characterized by increased expression of growth associated protein (GAP43) and synaptophysin—both markers for neuronal outgrowth—and increased amounts of tyrosine hydroxylase, suggesting an increase in innervation and a switch towards a more adrenergic phenotype (Nguyen et al., 2012; Ajijola et al., 2015; Li et al., 2015; Nakamura et al., 2016). Most studies, however, focus on the stellate ganglion, whereas limited information is available on the relevance of the other

ganglia providing sympathetic input to the heart. The superior cervical ganglion (SCG) gives input to the carotid plexus whose fibres run along the carotid arteries and provide sympathetic input towards the head where it stimulates parts of the eye, mouth and small blood vessels. The SCG also participates in innervation of the heart, providing the superior cardiac nerve that joins with postganglionic sympathetic fibres originating from other sympathetic ganglia at the cardiac plexus (Kawashima, 2005; Wink et al., 2020). Remarkably, in mice it has been shown that ganglionectomy of the SCG before MI leads to an almost entire loss of myocardial sympathetic innervation of the left ventricular anterior wall, in addition to a significantly reduction in chronic consequences of MI, such as myocardial inflammation, myocyte hypertrophy, and overall cardiac dysfunction (Ziegler et al., 2018). In human, it has been established that the SCG is involved in cardiac innervation (Kawashima, 2005), although the impact of a potential remodeling of this ganglion after MI, is unclear. In this respect, it may be relevant that the SCG is situated adjacent to the carotid body (CB), a small organ involved in oxygen, carbon and pH sensing, that has been shown to produce many neurotrophic factors (Lopez-Barneo et al., 2008). Of interest, Rocha et al. report that in rabbits the response of the chemo sensitive cardiac reflex of the CB was enhanced in the acute phase of MI (Rocha et al., 2003). Hypertonicity of the CB has been linked with cardiac disease such as hypertension and chronic heart failure. In rats with induced chronic heart failure, denervation of the CB performed early after MI, resulted in improved survival due to reduction of ventricular remodeling, less fibrosis and reduction of arrhythmias (Del Rio et al., 2013). Whether this is a transient phenomenon is unclear, as is the time-course of remodeling of the superior cervical ganglion and CB after MI.

Given the relevance of the SCG in cardiac innervation of the murine heart, as well as the still enigmatic role of this ganglion in the innervation of the human heart in health and disease, in the current study we investigated the remodeling of the murine SCG as well as the bordering CB over time after MI.

MATERIAL & METHODS

Animals

C57BL/6J (Jackson Laboratory) male mice of 13 weeks old (n=13) were used. All animal experiments were carried out according to the Guide for the Care and Use of Laboratory Animals published by NIH and approved by the Animal Ethics Committee of the Leiden University (License number AVD1160020185325), Leiden, The Netherlands.

Induction of MI and superior Cervical ganglia (SCG) isolation

Myocardial infarction was induced as previously described (Ge et al., 2020). Briefly, mice were anesthetized with 2% isoflurane, intubated and ventilated. The left anterior descending coronary artery (LAD) was permanently ligated and ischemia was confirmed by discoloration of the anterior wall of the left ventricle. The mice were given the analgesic drug Temgesic, 24 hours before and after the operation to relieve pain. As control, untreated mice (n=2) were included. All mice were maintained in a specific pathogen-free facility and regularly monitored. After 24h (n = 2; 4 SCG), 3 days (n = 3; 6 SCG), 7 days (n = 3; 6 SCG), or 6 weeks (n = 3; 6 SCG) post-MI mice as well as the healthy control mice (n=2; 4 SCG) were euthanized by CO2 asphyxiation (**Fig. 1A**). For dissection of the left- and right SCG, an incision was made in the skin of the neck area, the submandibular glands were moved aside, whereafter the carotid artery bifurcation with the SCG could be captured bilaterally. After excision, both SCG were fixed with 4% paraformaldehyde (104005; Merck Millipore), and embedded in paraffin.

Immunofluorescence staining of sympathetic ganglia

The schematic illustration **Fig. 1B** shows the workflow schedule, during which a series of 5 µm-thick paraffin sections throughout each ganglion were used for immunostaining and subsequently analyzed. The sections were deparaffinized, pre-treated with Tris-EDTA buffer (pH 9) at 98°C for 12 min for antigen retrieval, and incubated with the following neuronal antibodies: anti-tyrosine hydroxylase (TH, a marker for sympathetic nerves)(Fisher Scientific PA14679; 1:1000), anti-choline acetyltransferase (ChAT, considered a marker for parasympathetic nerves)(Abcam ab181023; 1:1000), and anti-β-tubulin III (Tubb3, general nerve marker)(Santa Cruz; SC-80005; 1:1000) overnight at 4°C. On the second day, the sections were incubated with secondary antibodies donkey anti-rabbit Alexa Fluor 488 (Invitrogen A-21206; 1:250), donkey anti-sheep Alexa Fluor 568 (Invitrogen A21099; 1:250) and donkey anti-mouse Alexa Fluor 647 (Invitrogen A31571; 1:250) for 1 hour and followed by a 10 min nuclear staining with DAPI (Invitrogen D3571: 1:1000). The slides were mounted with ProLong Gold Antifade Mountant (Invitrogen P36930) and the images were captured with the Zeiss AxioscanZ1 microscope slide scanner.

For quantification, a minimum of 10 sections throughout each ganglion was analyzed, by including every 5th section; in case of longitudinally sectioned ganglia, shorter intervals were applied. In order to select cells in an unbiased way, an 1 mm2 cross grid was placed with ImageJ on top of the image to aid in the random selection of cells for quantification (Fig.1-B1). When a cross overlapped at least ¾ with a cell, the region of interest (ROI) of the cytoplasm and nucleus was selected with ImageJ. After this was done for the whole section, the area of the

ROI template was applied to the TH and ChAT fluorescent channels of corresponding sections, after which the area of the cytoplasm and nucleus was measured with ImageJ.

To be able to quantify the dynamic remodeling of neurons in the area adjacent to the carotid body vs. the area remote from the carotid body, three images per ganglion were selected (4 ganglia per time point) that contained the CB adjacent to the SCG (Fig. 1-B2). Three images per ganglion that contained SCG area remote to the CB were also selected (Fig. 1-B2). Using ImageJ software (version 1.52p), a 500 x 500 um square was placed within the SCG adjacent to the CB and in the remote region of the SCG. Within each square 20 cells were drawn in as ROI and the area and ChAT intensity were measured in ImageJ (version 1.52p).

Immunofluorescence detection and quantification of neurotrophic factors

5 µm-thick paraffin sections that contained the SCG adjacent to the CB were used for the study of neurotrophic factors (Fig. 1-B2). As described above, the sections were first deparaffinized and antigen retrieval was performed. Hereafter, the sections were incubated with the neurotrophic markers anti-brain derived neurotrophic factor (BDNF)(Abcam ab108319; 1:250, anti-nerve growth factor (NGF)(Abcam ab6199; 1:100) or the receptor anti-pan Neurotrophic Receptor Tyrosine Kinase (pan TrK)(Abcam ab181560; 1: 500) combined with anti-TH (Fisher Scientific PA14679; 1:1000) overnight at 4°C. Secondary antibodies, donkey anti-rabbit Alexa Fluor 488 (Invitrogen A-21206; 1:250) and donkey anti-sheep Alexa Fluor 568 (Invitrogen A21099; 1:250), were incubated to visualize the expression of corresponding factors and receptor, followed by a 10 min nuclear staining with DAPI (Invitrogen D3571: 1:1000).

Images were captured with Leica confocal SP8 microscopy under the same exposure time and gain settings. To quantify BDNF, NGF and pan-TrK expression, 3 sections of each ganglion and 4 ganglia of each timepoint were used to measure the corresponding fluorescence intensity in ImageJ (version 1.52p).

Immunohistochemical staining of growth-associated protein 43 and quantification

5 µm-thick paraffin sections were used to study neuronal remodeling using the Growth Associated Protein 43 (GAP43), a marker for nerve sprouting (Benowitz and Routtenberg, 1997; Korshunova and Mosevitsky, 2010) (Fig. 1-B3). As previously described, the sections were first deparaffinized and antigen retrieval was performed. Hereafter, the sections were incubated with the primary recombinant anti-GAP43 antibody (Abcam ab75810, 1:2000) overnight at 4°C. The next day, the primary antibody was washed away and thereafter the slides were incubated with the secondary biotinylated anti-rabbit IgG (H+L) antibody (Vector Laboratories BA-1000, 1:200) for 1 hour, followed by an incubation with ABC-AP (Vector Laboratories AK-5000) for 30 min. To visualize GAP43, the slides were incubated with alkaline phosphatase substrate

(Vector Laboratories SK-5105) in the dark for 5 minutes. The substrate was then washed away and the slides were counterstained with haematoxylin (Klinipath VWRK4085-9002) to visualize the nuclei. After dehydration the sections were mounted with Entellan (Merck 107961) mounting medium and all images were captured with the 3DHISTECH scanner.

To quantify GAP43 expression, 3 sections of each ganglion and 4 ganglia per time point were quantified. Individual sections were imported into ImageJ and the ganglion region was selected by hand with ImageJ selection function and set as ROI. To acquire the percentage of the GAP43+ area the measurements were performed as follows: within the green channel the total area of the ganglion was measured by setting the threshold on the maximum and the GAP43+ area was measured using the default threshold in ImageJ (version 1.52p).

Statistics

Data were presented as mean ± standard error of the mean (SEM). One-way ANOVA and multiple comparisons followed by a Tukey's post hoc analysis or Dunnett's T3 multiple comparisons test when standard deviations (SDs) are different to determine statistically significant differences among groups. To compare the differences of neuronal cell size and ChAT intensity in the neuronal cells located adjacent versus remote to CB, the paired t-test was applied. Results were considered significantly different when the p value was <0.05. GraphPad Prism (GraphPad Software, San Diego, CA, USA; version 9) was used for statistical analysis. Pearson correlation coefficients were used to test the linear relationship between two variants. R (version 4.0.2) was used for Pearson correlation coefficients and linear regression.

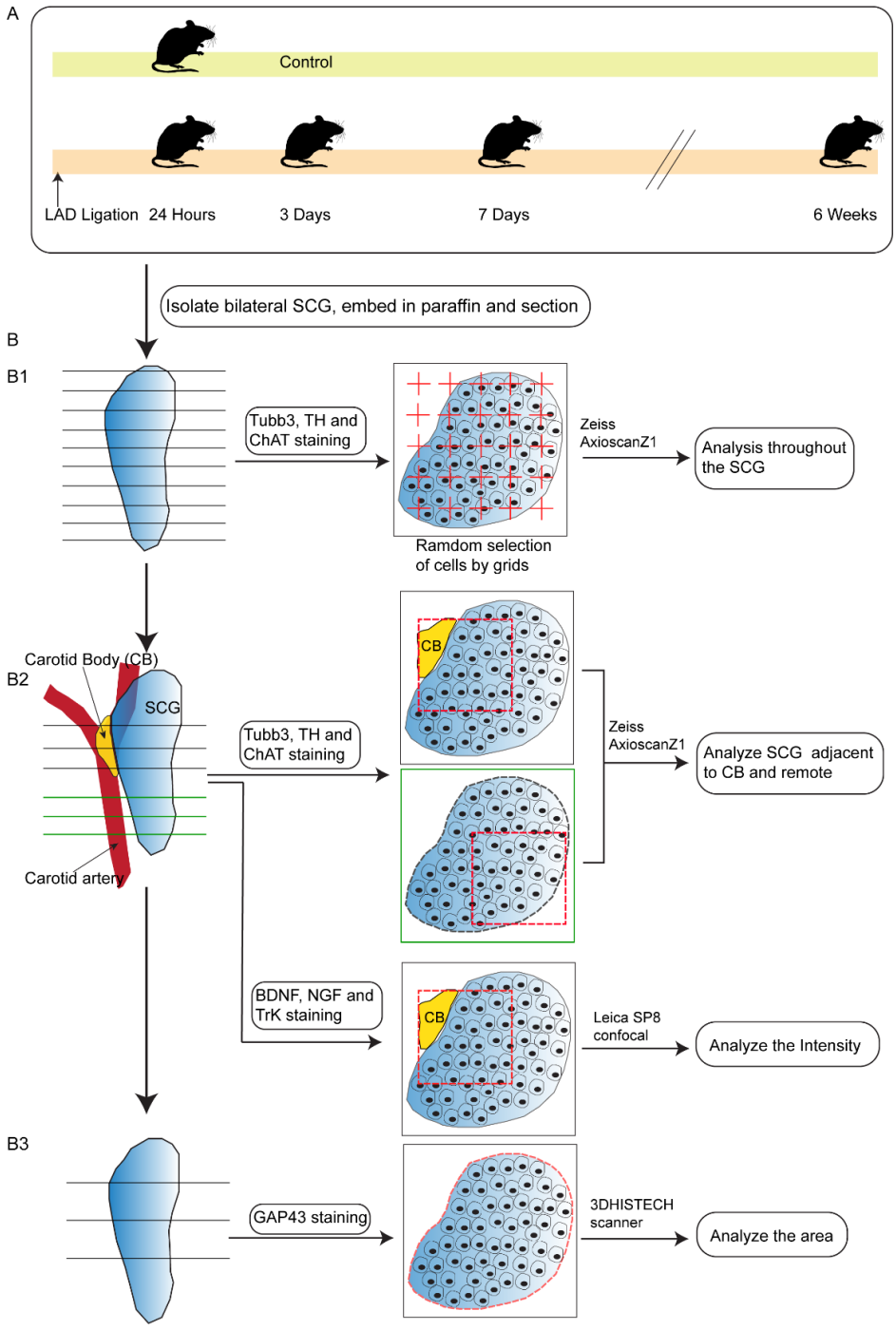
A
Control
LAD Ligation
24 Hours
3 Days
7 Days
6 Weeks
Isolate bilateral SCG, embed in paraffin and section
B
B1
Tubb3, TH and ChAT staining
Ramdom selection of cells by grids
Zeiss AxioscanZ1
Analysis throughout the SCG
Carotid Body (CB)
B2
SCG
Carotid artery
Tubb3, TH and ChAT staining
CB
Zeiss AxioscanZ1
Analyze SCG adjacent to CB and remote
BDNF, NGF and TrK staining
CB
Leica SP8 confocal
Analyze the Intensity
B3
GAP43 staining
3DHISTECH scanner
Analyze the area

Figure 1. Schematic workflow of the time-course study. From the top to the bottom panels, the schematic diagram is a step-by-step illustration of the methods performed in this time-course study of SCG remodeling after MI. A. Representation of MI induction and the post-MI timepoints in mouse. B. Brief illustration of all study methods applied. Left panels display an overview of the sections chosen in each analysis. The midline panels explain the cells/regions selection for each analysis from a cross-sectioned view. B1. Analysis of ChAT and TH expression in complete SCG. B2. Analysis of ChAT and TH expression in the region adjacent versus remote to the CB. Quantification of neurotrophic factors and their receptors in the region adjacent to the CB. B3. Analysis of growth associated protein 43 (GAP43) in the SCG.

RESULTS

Superior cervical ganglia exhibit dynamic neuronal remodeling after acute myocardial infarction

To investigate the remodeling of the murine SCG over time post-MI, MI was induced in mice by permanent ligation of the LAD and the SCG was analyzed after 24 hours, 3 days, 7 days, and 6 weeks. Staining of serial sections of the murine SCG with the general nerve marker Tubb3 provided an overview of the distribution of neurons and nerves in each ganglion (Fig. 2A). Previous studies in sympathetic ganglia (i.e. stellate ganglia) in both rat and pig demonstrated the existence of ChAT+ neurons in sympathetic ganglia (Nguyen et al., 2012; Ajijola et al., 2015). We performed immunostainings for the parasympathetic marker ChAT as well as with the sympathetic TH marker in the SCG post-MI. This revealed a series of striking alterations in SCG neuronal cells in the different stages after MI compared to control SCG, referred to as dynamic neuronal remodeling. As shown in Fig. 2A, we observed many neuronal cells that expressed both TH and ChAT (TH+ ChAT+) in the SCG throughout the post-MI timeline.

Multiple control experiments were carried out to confirm the reliability of the detected TH+ChAT+ expression in murine SCG neuronal cells. Double immunostaining for ChAT and TH was performed on the nodose ganglion (NG), a well-described entirely parasympathetic ganglion. As reported by Bookout et. al (Bookout and Gautron, 2021), neuronal cells of the NG were only positive for ChAT, but not for TH (TH-ChAT+), and both TH- and TH+ neuronal cells were observed in the "bridge" between the NG and the SCG (Supplemental Fig. 1A). Moreover, no obvious difference in ChAT intensity was detected between the NG and SCG neuronal cells (Supplemental Fig. 1A). In addition, immunoblot analysis of protein lysates from either whole SCG tissue or nuclei showed the main presence of ChAT at the size of 69KDa as expected (Supplemental Fig. 1B and C), which reconfirmed the specific detection of ChAT in SCG. The cell lysate of non-neuronal cells (human epicardial cells) was used as negative control, due to the absence of ChAT expression in these cells. (Supplemental Fig. 1C). These findings indicate that no cross reaction between ChAT and TH occurred in the double immunostainings, and

support the specificity of the ChAT staining. Co-staining of TH and ChAT in a human sympathetic ganglion (stellate ganglion) presented with a similar ChAT staining pattern as observed in the mouse ganglia (Supplemental Fig. 1D).

Time course comparison of the SCG of healthy control mice vs. post-MI mice revealed obvious alterations of the ChAT expression in neuronal cells both in the level of expression as well as the intracellular location in the neuronal cell body. Quantification of the neuronal cell size of the entire SCG indicated that neuronal remodeling appears as early as 3 days post-MI and shows a significant increase at day 7 post-MI when compared to control animals (Fig. 2B). TH expression was steadily high throughout the timeline (Fig. 2C) whereas ChAT expression decreased as early as 24 hours post-MI, showed a significant decrease at day 7 post-MI as compared to control, and had returned to control values after 6 weeks post-MI (Fig. 2D). This alteration in ChAT expression is concomitant with a significant decrease of ChAT expression in the nuclei, with the most marked decrease at day 7 post-MI (Fig. 2E).

SCG neurons adjacent to the CB display robust neuronal enlargement

The most striking neuronal cell remodeling was observed in the region of the SCG most adjacent to the CB in post-MI mice. Therefore, further time course analysis was performed specifically of this region. As presented in Fig. 3A, post-MI SCG neuronal cells located adjacent to the CB exhibit an striking enlargement in cell size accompanied with a loss of ChAT expression, especially at day 3 post-MI, compared to a relatively even distribution in cell size and ChAT expression of control SCG. Pairwise presented data in Supplemental Fig. 2A and B show the distribution width of the neuronal cell size and ChAT intensity, indicating a varying degree of remodeling within each time point as well as the region within the post-MI SCG. When observing the changes over time, the alterations in the neuronal cells adjacent to the CB versus the neuronal cells located remotely demonstrated a clear remodeling, with a significant difference ($P < 0.01$) of the change in cell size (Fig. 3B). The ChAT intensity of the neuronal cells adjacent to the CB versus the neuronal cells located remotely was not significantly different (Fig. 3C).

As the enlarged neuronal cells displayed low expression of ChAT, especially a decrease in cytoplasmic ChAT 3 days post-MI (Fig. 3A-C), co-efficiency analysis was performed, to examine whether the cell enlargement caused the decrease of ChAT. This revealed a negative correlation between neuronal cell size and ChAT expression, which was significantly detectable in the SCG 24 hours, 3 days and 7 days post-MI (Fig. 3D). The correlation disappeared in SCG 6 weeks post-MI (Fig. 3D).

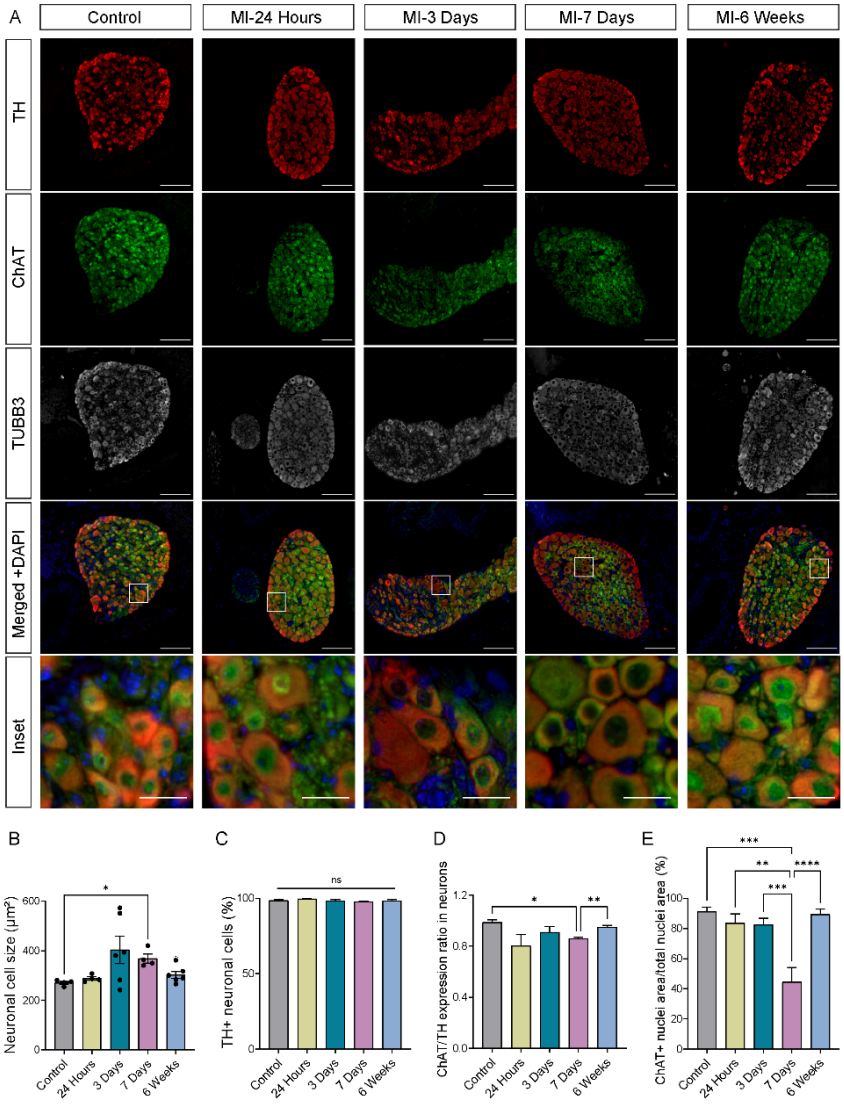

Figure 2. Superior cervical ganglia exhibit dynamic remodeling after MI. A. Immuno-fluorescence staining of TH (red), ChAT (green), Tubb3 (gray), and nuclei (blue) in SCG from control mice and mice post-MI at 24 hours, 3 days, 7 days, and 6 weeks. The enlarged regions are shown at the bottom panels. Scale bar = 100 µm in all panels, with exemption of the enlarged panels: here Scale bar = 20 µm. B. Average size of TH+ cells of each ganglion derived from control mice and post-MI mice at 24 hours, 3 days, 7 days, and 6 weeks. C. Percentage of sympathetic neurons that show high TH expression in all ganglia. D. Comparison of the area ratio of ChAT expression/TH expression in the SCG neuronal cells of each timepoint. E. Comparison of the expression of ChAT in neuronal nuclei in each timepoint. ns = not significantly different, * P< 0.05, ** P< 0.01, *** P<0.001, **** P< 0.0001.

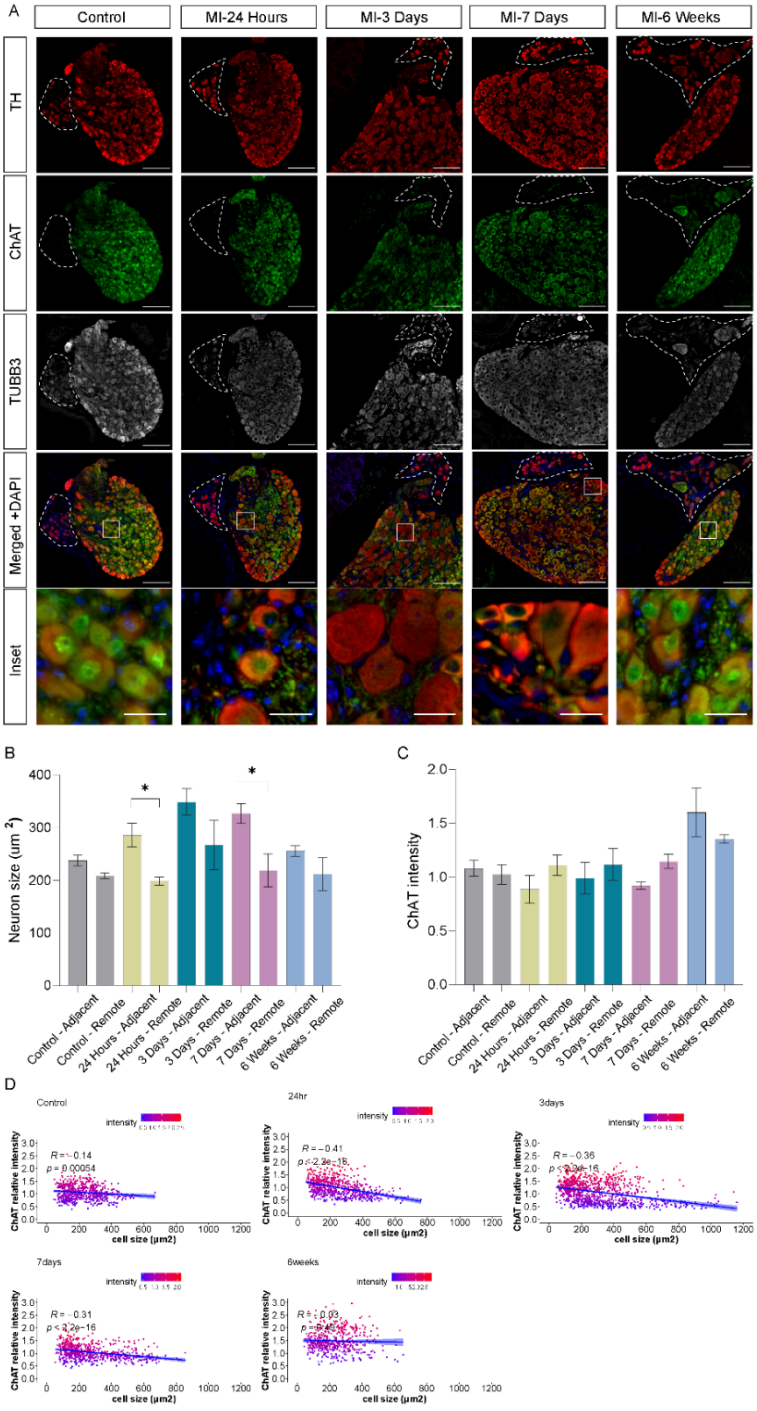
A
Control
MI-24 Hours
MI-3 Days
MI-7 Days
MI-6 Weeks
TH
ChAT
TUBB3
Merged +DAPI
Inset
B
Neuron size (um 2)
Control - Adjacent
Control - Remote
24 Hours - Adjacent
24 Hours - Remote
3 Days - Adjacent
3 Days - Remote
7 Days - Adjacent
7 Days - Remote
6 Weeks - Adjacent
6 Weeks - Remote
C
ChAT intensity
D
Control
24hr
3days
7days
6weeks
ChAT relative intensity
cell size (µm2)
intensity

Figure 3. SCG neurons adjacent to the carotid body display robust neuronal enlargement. A. Immunofluorescence staining of TH (red), ChAT (green), Tubb3 (gray), and nuclei (blue) in SCG regions located adjacent to the CB (dashed lines) of control mice and post-MI mice at 24 hours, 3 days, 7 days, and 6 weeks. Enlarged region is shown at the bottom panels. Scale bar = 100 μm all panels, except in the enlarged panel, where Scale bar = 20 μm. B and C. Bar graphs that display the alterations of SCG neuronal cell size and the relative ChAT intensity in the region *adjacent* to the CB vs *remote*. D. ChAT intensity of neuronal cells are plotted against the neuronal cell size (μm^2) of SCG derived from control mice and post-MI mice at 24 hours, 3 days, 7 days, and 6 weeks. The lines indicate the linear regression of the plotted data. Light blue regions indicate the standard error of the mean (SEM) of ChAT intensity. Each point represents one neuronal cell. R demonstrates correlation coefficients at indicated P value. ** P<0.01.

BDNF and NGF expression is increased in CB and neuronal cells after MI

Based on our observation that SCG neurons adjacent to the CB exhibited stronger remodeling post-MI, and as it has been shown that the CB type I glomus cells can be identified with the conventional marker TH and that these cells secrete neurotrophic factors during development as well as in response to environmental stimuli (Pulgar-Sepúlveda et al., 2018; Stocco et al., 2020), as a next step we assessed BDNF expression in the SCG and the CB. In the CB, glomus type I cells were recognized as TH+ cells, and analysis of BDNF expression indicated an increased expression of BDNF in type I glomus cells (i.e. TH+ cells) of the CB post-MI, which reached its highest peak and showed a significant difference at day 7 post-MI when compared to control (Fig. 4A and B). Notably, BDNF expression in the CB was significantly regressed at week 6 compared to day 7 post-MI, and returned to basal level (Fig. 4B).

In addition to BDNF, NGF, another well-known neurotrophic factor, was examined in both the CB and SCG neurons. Similar to BDNF, NGF expression in both the CB and SCG neurons reached the first small peak 24 hours post-MI, although not statistically significantly different from control due to the high variation (Fig. 5A-C). The second peak of NGF expression appeared at day 7 post-MI and the expression was significantly increased as compared to SCG neurons in control, followed by a drop 6 weeks post-MI (Fig. 5A-C).

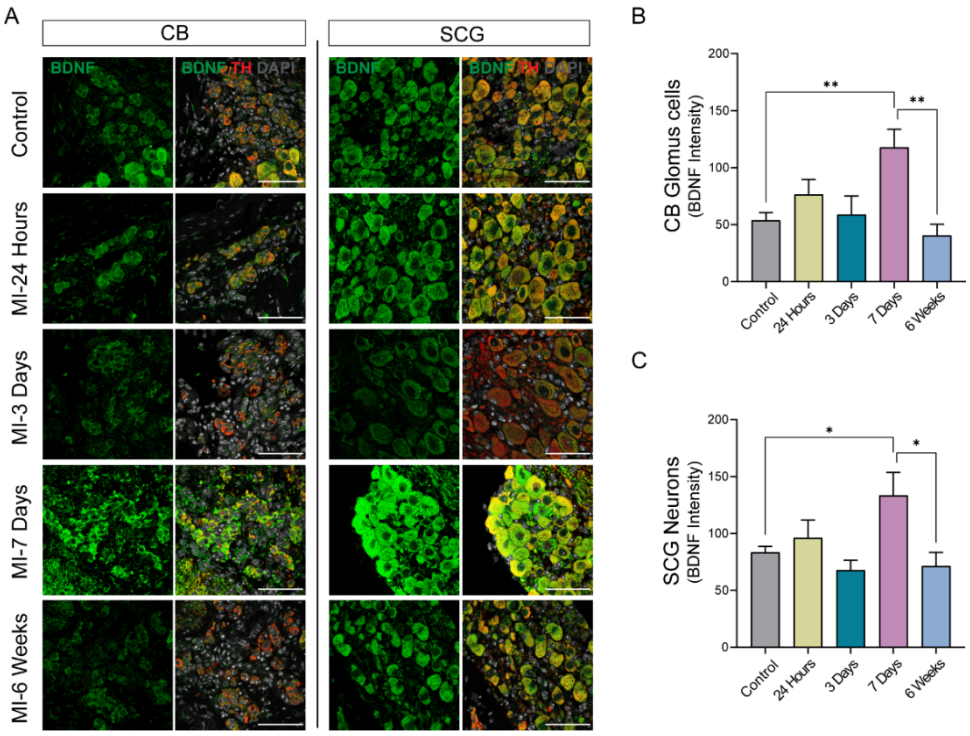

Figure 4. BDNF is increased in CB and neurons in SCG after MI. A. Immunofluorescence staining of BDNF (green), TH (red), and nuclei (DAPI, gray) in the CB and SCG neurons of control mice and mice post-MI at 24 hours, 3 days, 7 days, and 6 weeks. Scale bar = 100 µm. B and C. BDNF intensity of the CB and SCG neurons at different timepoints post-MI were quantified by measuring fluorescence integrated density. Both the CB glomus type I cells and SCG neurons are recognized as TH^+ cells. * $P< 0.05$, ** $P< 0.01$

High affinity receptors of BDNF and NGF in SCG neurons are increased after MI

Given the importance of the neurotrophic receptor (TrKA and TrKB) expression in neurons to facilitate the binding of neurotrophic factors (NGF and BDNF) and mediating their subsequent impact on neuronal survival and axonal growth (Ginty and Segal, 2002; Kuruvilla et al., 2004; Kimura et al., 2012), we investigated whether the high affinity receptors TrKA and TrKB were expressed in the SCG. Immunostaining of SCG, using a pan-TrK antibody, showed a low expression of TrK in control SCG neurons (**Fig. 6A**). According to the time course analysis, TrK expression in SCG neurons gradually increased and was significantly upregulated at day 7 post-MI. This upregulation, when compared to control, was still present at 6 weeks post-MI (**Fig. 6A and B**).

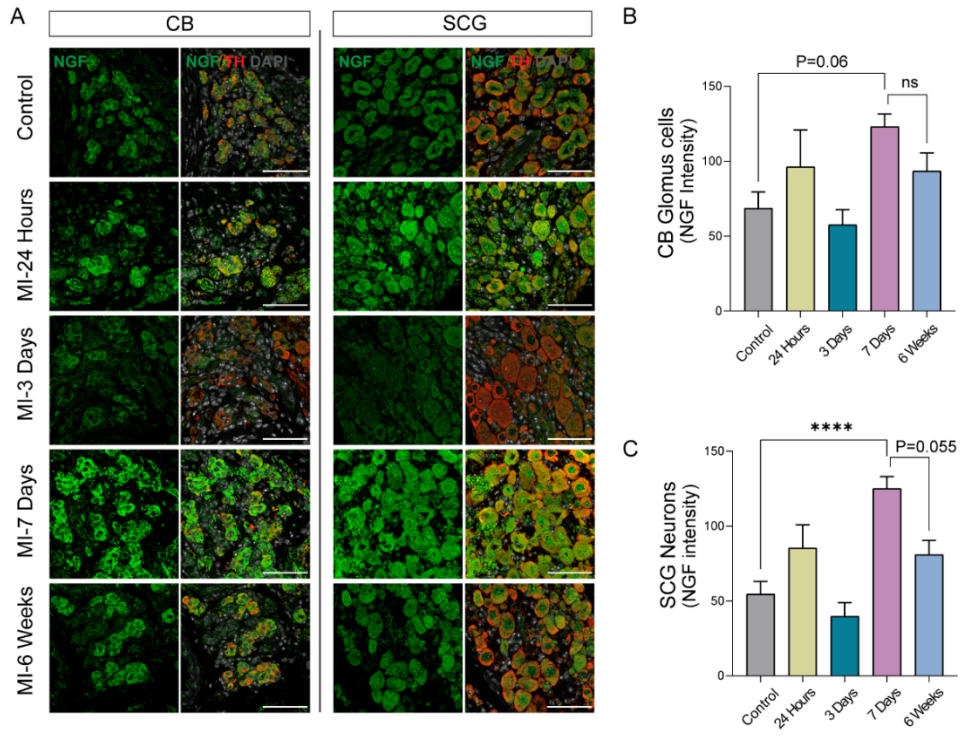

Figure 5. NGF is increased in CB and neurons in SCG after MI. A. Immunofluorescence staining of NGF (green), TH (red), and nuclei (DAPI, grey) in the CB and SCG neurons of healthy control mice and mice post-MI at 24 hours, 3 days, 7 days, and 6 weeks. Scale bar = 100 µm. B and C. NGF intensity of the CB and SCG neurons at different timepoints post-MI were quantified by measuring fluorescence integrated density. Both the CB glomus cells and SCG neurons are recognized as TH^+ cells. **** P< 0.0001.

GAP43 reveals neuronal outgrowth after MI

As we observed neuronal remodeling concomitant with an increased expression of the neurotrophic factors BDNF and NGF and their receptors, we postulated that this neuronal remodeling in SCG after MI mediates new axon formation and axonal elongation. SCG of control mice and mice post-MI were therefore immunostained for GAP43, a growth- and plasticity-related protein that is involved in axon elongation during early development and nerve regeneration (Holahan, 2017). As is shown in **Fig. 7A**, after MI, a very strong increase in GAP43 expression was observed in axons and, to a lesser extent, also inside the neuronal cell bodies, while in the control SCG a very low number of axons expressed GAP43. Time-course comparison indicated a significant upregulation of GAP43 expression at all examined time points after MI, with the highest peak at day 3 post-MI (**Fig. 7B**).

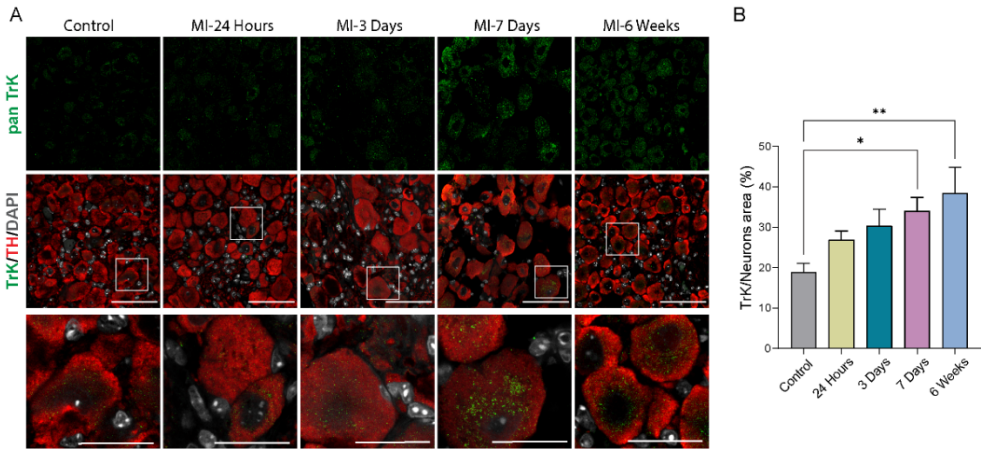

Figure 6. Increase in high affinity receptors for BDNF and NGF in SCG neurons after MI. A. Immunofluorescence staining of pan-Trk (green), TH (red), and nuclei (DAPI, gray) in SCG of control mice and mice post-MI at 24 hours, 3 days, 7 days, and 6 weeks. Representative images are shown in upper 2 panels and enlarged images in the lowest panels. Scale bar = 100 µm. Scale bar = 20 µm in enlarged panels. B. Time-course comparison of TrK expression in SCG. Percentage of TrK^+ area out of the TH^+ neuronal area is used to indicate TrK expression level.* P< 0.05, ** P< 0.01.

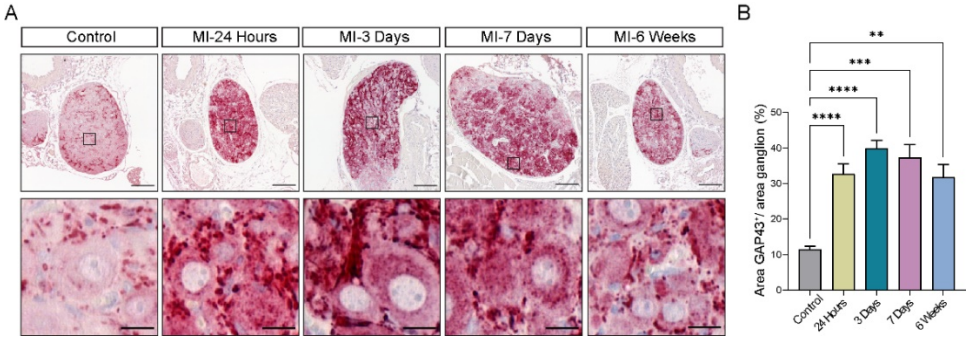

Figure 7. Growth Associated Protein 43 reveals neuronal outgrowth after MI. A. Representative images of immunohistochemistry staining of GAP43 in SCG from control mice and mice post-MI at 24 hours, 3 days, 7 days, and 6 weeks. Scale bar = 100 µm. Lower panels are enlarged images, scale bar = 20 µm . B. Time-course comparison of the GAP43 expression in SCG, percentage of GAP43+ area out of the ganglionic area is used to indicate the GAP43 expression level. ** P< 0.01, *** P<0.001, **** P< 0.0001.

DISCUSSION

The role of the autonomic nervous system in post-MI arrhythmogenicity has gained increased attention over the past decades. Whereas vagal innervation is considered cardioprotective, sympathetic overdrive is associated with arrhythmias and sudden cardiac death (Fukuda et al., 2015; Hausenloy et al., 2019). Remarkably, although nerve tissue is generally notorious for its lack of regeneration capacity in adults, after cardiac damage the intriguing phenomenon of cardiac sympathetic hyperinnervation has been reported in multiple animal species, suggesting a renewed capacity of neuronal outgrowth of sympathetic neurons (Cao et al., 2000; Yokoyama et al., 2017). In line with this, several studies in human, rat, rabbit and pig, indicated neuronal and electrical remodeling in the stellate ganglia after MI (Ajijola et al., 2012; Han et al., 2012; Nguyen et al., 2012; Ajijola et al., 2015). In addition to the stellate ganglion and upper thoracic ganglia, the cardiac plexus also receives contributions from sympathetic nerves derived from the SCG that participate in cardiac ventricular innervation in both human and mouse (Pather et al., 2003; Kawashima, 2005; Ziegler et al., 2018). However, in contrast to the stellate ganglion, data on the time course of neural remodeling in the SCG - that is in close proximity to the oxygen- and PH-sensing CB - after MI is still limited. In the current study, we assessed the neuronal remodeling of murine entire SCG, including the CB, at several time points post-MI.

Our key findings are: i) Both ChAT and TH are co-expressed in SCG neuronal cells in healthy mice; ii) After MI, remodeling of the SCG occurs, with an increased size of ganglionic cells and a decreased intensity of ChAT expression; iii) Neuronal remodeling in the SCG starts already 24 hours after MI, reaches a peak at day 7 post-MI, after which a return to the healthy control situation is observed within 6 weeks post-MI; iv) The most robust neuronal remodeling of the SCG takes place at the region adjacent to the CB; v) An increase of neurotrophic factors (BDNF and NGF) occurs in the CB and neuronal cells, in the latter accompanied by a dynamic increase in the high affinity receptors of BDNF and NGF, concomitant with vi) an increase in axonal outgrowth in the SCG.

Expression of nerve markers - noticeable expression of ChAT in SCG. Sympathetic neuronal cells are generally considered as adrenergic cells, expressing the rate-limiting enzyme TH, that plays a pivotal controlling role in the synthetic pathway of catecholamines (adrenergic neurotransmitters) (Kobayashi and Nagatsu, 2012). In contrast, ChAT, the enzyme that catalyzes the synthesis of acetylcholine (cholinergic neurotransmitter in the peripheral nervous system) (Deutch and Roth, 2004) is generally considered as a marker for parasympathetic neurons. Remarkably, we observed neuronal cells that both express TH and ChAT in the mouse SCG. While we did observe TH+ChAT- in 3 days post-MI SCG and CB glomus type I cells, we did not detect TH in the parasympathetic nodose ganglion, indicating adequate

specificity of the antibody. In addition, this was supported by the detection of ChAT in different intracellular locations, either both in the cytoplasm and the nucleus or only in the cytoplasm, in SCG at different timepoints post-MI. Enriched biphenotypic neurons (ChAT+TH+) were also observed in human sympathetic ganglia in the current study. This is in contrast with what has been found in rat and pig sympathetic ganglia, where only few neurons are either biphenotypic or ChAT+ (Anderson et al., 2006; Ajijola et al., 2015), and no ChAT+ neurons were observed in rabbit sympathetic ganglia (Nguyen et al., 2012). These data indicate that phenotype differences might exist in sympathetic neurons among species, and the mouse model seems to resemble human ganglia in this respect, thus holding potential as an adequate model to study transdifferentiation (i.e. switch in neuronal phenotype) after cardiac damage (Olivas et al., 2016).

Neuronal remodeling. Post-MI time-course analysis demonstrated a neuronal remodeling of SCG which presented as a gradual decrease of ChAT expression and SCG neuronal cell enlargement with a remodeling starting already after 24 hours with a peak on day 7 and regression towards the control situation 6 weeks post-MI. These findings are in accordance with cardiac sympathetic re- and hyper-innervation post-MI (Kimura et al., 2007; Yokoyama et al., 2017). At the peak of remodeling on day 7 we observed a loss of nuclear ChAT. In both human and mouse it has been found that in younger subjects, ChAT was found mostly in neuronal nuclei whereas ChAT expression increased in neuronal cytoplasm in older individuals (Gill et al., 2007; Albers et al., 2014). We speculate that the stress response upon MI might induce a loss of nuclear ChAT, similar as seen with aging. It has previously been reported that the 69-kDa ChAT isoform can shift between the cytoplasmic and nuclear compartments, and nuclear ChAT can act as a transcriptional activator of a high affinity choline transporter (CHT1) which also regulates acetylcholine synthesis in neurons (Matsuo et al., 2011). The nuclear localization has also been shown to induce an epigenetic response (Winick-Ng and Rylett, 2018), which might also further mediate neuronal remodeling seen in SCG upon MI.

Neurotrophic factors & role CB. The finding that robust neuronal remodeling occurred in SCG neurons adjacent to the CB, suggests that the remodeling is potentially mediated by the CB. The CB, a neural crest derived structure located at the carotid bifurcation, is the main peripheral chemoreceptor in mammals (Pulgar-Sepúlveda et al., 2018). It can sense and respond to changes in blood flow, O2- and CO2 levels, PH as well as changes in metabolites such as glucose and lactate (Lopez-Barneo et al., 2008; Ortega-Saenz and Lopez-Barneo, 2020). In the CB, the type I glomus cells, that are immunoreactive for TH, express a wide range of growth factors and neurotrophic factors during development (Stocco et al., 2020). In our time-course analysis, after MI an increase in expression of neurotrophic factors (BDNF and NGF) in the type I glomus cells was observed. Of note, the peak of neuronal remodeling occurred when

highest levels of BDNF and NGF were expressed in the CB. Moreover, an upregulation of the TrK (the high affinity receptors of BDNF and NGF) receptor in the SCG neurons was observed alongside the upregulation of BDNF and NGF expression post-MI. This response was accompanied with neuronal cell enlargement and a decrease of ChAT expression. Surprisingly, levels of BDNF and NGF expression did not return to control levels at 6 weeks post-MI, whereas also the TrK expression in SCG neurons was maintained at high levels with a significant difference compared to control (Fig. 5B). Results indicate that neuronal remodeling is influenced by neurotrophic factors via a paracrine and autocrine effect, as was previously described (Davies, 1996; Cheng et al., 2011).

Although remodeling indicates a change in phenotype, the question is whether this actually contributed to an increase in new axons from the SCG. GAP43, a growth-associated protein, participates in the developmental regulation of axonal growth and the formation of new synapses, neurite outgrowth, and synaptogenesis after injury (Hou et al., 1998; Nguyen et al., 2009; Holahan, 2015). This might be related to its function in growth cones by stabilizing f-actin, preventing actin polymerization and promoting microtubule-based neurite outgrowth (He et al., 1997; Nguyen et al., 2009; Kusik et al., 2010). As its transcriptional expression is up-regulated in differentiating and regenerating neurons, though lowly expressed in mature neurons (Skene, 1989), it is a suitable marker to examine the neo-outgrowth of nerves after damage. In addition to previous findings of GAP43 expression in sprouting axons in infarcted heart (Zhou et al., 2004), in the current study, we showed a striking upregulation of the GAP43 expression in SCG neurons and axons post-MI, starting from as early as 24 hours post-MI compared to control.

In conclusion, overt remodeling towards an increased adrenergic phenotype occurs in the SCG as well as in the area of the CB, accompanied with an increase in axonal outgrowth in the SCG. The dynamics in expression of neurotrophic factors and their high affinity receptors, indicate a paracrine/autocrine neurotrophic effect. Results suggest an interaction of the SCG and CB after MI, that might contribute to pathological cardiac sympathetic hyperinnervation.

FUTURE PERSPECTIVES

In this time-course study, we show that the cholinergic marker ChAT is also expressed in SCG sympathetic neurons of the SCG and that expression of ChAT displays a dynamic transition, from expression in both cytoplasm and nucleus to only in cytoplasmic expression after MI. Further studies are required to study the functional implication of ChAT in adrenergic neurons and the mechanisms behind ChAT dynamic change caused by MI. Taking into account that the CB participates in SCG neuronal remodeling, as was indicated in the present study, the further

exploit of the potential interaction between CB and SCG could empower our integrative understanding of cardiac innervation after damage.

AUTHOR CONTRIBUTIONS

All authors contributed to the study conception and design. The experiments were designed by Y.G. and M.R.M.J. and performed by Y.G and L.v.R.. Data collection and analysis were performed by Y.G. and L.v.R., supervised by J.M.v.G and M.R.M.J, The first draft of the manuscript was written by Y.G., L.v.R, J.M.v.G. and M.R.M.J. and all authors commented on previous versions of the manuscript. All authors read and approved the final manuscript.

ACKNOWLEDGMENTS

We are grateful to Tessa van Herwaarden (Department of Cell and Chemical Biology, LUMC, Leiden, the Netherlands) for her help with induction of MI.

FUNDING

This work is supported by the Netherlands Organization for Scientific Research (NWO) [016.196.346 to M.R.M.J.], the Dutch Heart Foundation [2017T059 to A.M.S].

DECLARATION OF COMPETING INTEREST

The authors declare no competing interests.

REFERENCES

Ajijola, O.A., Wisco, J.J., Lambert, H.W., Mahajan, A., Stark, E., Fishbein, M.C., et al. (2012). Extracardiac Neural Remodeling in Humans With Cardiomyopathy. 5(5), 1010-1116. doi: doi:10.1161/CIRCEP.112.972836.

Ajijola, O.A., Yagishita, D., Reddy, N.K., Yamakawa, K., Vaseghi, M., Downs, A.M., et al. (2015). Remodeling of stellate ganglion neurons after spatially targeted myocardial infarction: Neuropeptide and morphologic changes. Heart Rhythm 12(5), 1027-1035. doi: 10.1016/j.hrthm.2015.01.045.

Albers, S., Inthathirath, F., Gill, S.K., Winick-Ng, W., Jaworski, E., Wong, D.Y., et al. (2014). Nuclear 82-kDa choline acetyltransferase decreases amyloidogenic APP metabolism in neurons from APP/PS1 transgenic mice. Neurobiol Dis 69, 32-42. doi: 10.1016/j.nbd.2014.05.008.

Anderson, C.R., Bergner, A., and Murphy, S.M. (2006). How many types of cholinergic sympathetic neuron are there in the rat stellate ganglion? Neuroscience 140(2), 567-576. doi: https://doi.org/10.1016/j.neuroscience.2006.02.021.

Benowitz, L.I., and Routtenberg, A. (1997). GAP-43: an intrinsic determinant of neuronal development and plasticity. Trends Neurosci 20(2), 84-91. doi: 10.1016/s0166-2236(96)10072-2.

Bookout, A.L., and Gautron, L. (2021). Characterization of a cell bridge variant connecting the nodose and superior cervical ganglia in the mouse: Prevalence, anatomical features, and practical implications. Journal of Comparative Neurology 529(1), 111-128. doi: 10.1002/cne.24936.

Cao, J.M., Chen, L.S., KenKnight, B.H., Ohara, T., Lee, M.H., Tsai, J., et al. (2000). Nerve sprouting and sudden cardiac death. Circ Res 86(7), 816-821. doi: 10.1161/01.res.86.7.816.

Cheng, P.-L., Song, A.-H., Wong, Y.-H., Wang, S., Zhang, X., and Poo, M.-M. (2011). Self-amplifying autocrine actions of BDNF in axon development. Proceedings of the National Academy of Sciences 108(45), 18430. doi: 10.1073/pnas.1115907108.

Davies, A.M. (1996). Paracrine and autocrine actions of neurotrophic factors. Neurochemical Research 21(7), 749-753. doi: 10.1007/BF02532296.

de Bakker, J.M., van Capelle, F.J., Janse, M.J., Tasseron, S., Vermeulen, J.T., de Jonge, N., et al. (1993). Slow conduction in the infarcted human heart. 'Zigzag' course of activation. Circulation 88(3), 915-926. doi: 10.1161/01.cir.88.3.915.

Del Rio, R., Marcus, N.J., and Schultz, H.D. (2013). Carotid chemoreceptor ablation improves survival in heart failure: rescuing autonomic control of cardiorespiratory function. J Am Coll Cardiol 62(25), 2422-2430. doi: 10.1016/j.jacc.2013.07.079.

Deutch, A.Y., and Roth, R.H. (2004). "CHAPTER 9 - Pharmacology and Biochemistry of Synaptic Transmission: Classic Transmitters," in From Molecules to Networks, eds. J.H. Byrne & J.L. Roberts. (Burlington: Academic Press), 245-278.

Fukuda, K., Kanazawa, H., Aizawa, Y., Ardell, J.L., and Shivkumar, K. (2015). Cardiac innervation and sudden cardiac death. Circ Res 116(12), 2005-2019. doi: 10.1161/circresaha.116.304679.

Ge, Y., Smits, A.M., Van Munsteren, J.C., Gittenberger-De Groot, A.C., Poelmann, R.E., Van Brakel, T.J., et al. (2020). Human epicardium-derived cells reinforce cardiac sympathetic innervation. Journal of Molecular and Cellular Cardiology 143, 26-37. doi: 10.1016/j.yjmcc.2020.04.006.

Gill, S.K., Ishak, M., Dobransky, T., Haroutunian, V., Davis, K.L., and Rylett, R.J. (2007). 82-kDa choline acetyltransferase is in nuclei of cholinergic neurons in human CNS and altered in aging and Alzheimer disease. Neurobiol Aging 28(7), 1028-1040. doi: 10.1016/j.neurobiolaging.2006.05.011.

Ginty, D.D., and Segal, R.A. (2002). Retrograde neurotrophin signaling: Trk-ing along the axon. Curr Opin Neurobiol 12(3), 268-274. doi: 10.1016/s0959-4388(02)00326-4.

Han, S., Kobayashi, K., Joung, B., Piccirillo, G., Maruyama, M., Vinters, H.V., et al. (2012). Electroanatomic remodeling of the left stellate ganglion after myocardial infarction. J Am Coll Cardiol 59(10), 954-961. doi: 10.1016/j.jacc.2011.11.030.

Hausenloy, D.J., Bøtker, H.E., Ferdinandy, P., Heusch, G., Ng, G.A., Redington, A., et al. (2019). Cardiac innervation in acute myocardial ischaemia/reperfusion injury and cardioprotection. Cardiovascular Research 115(7), 1167-1177. doi: 10.1093/cvr/cvz053.
He, Q., Dent, E.W., and Meiri, K.F. (1997). Modulation of actin filament behavior by GAP-43 (neuromodulin) is dependent on the phosphorylation status of serine 41, the protein kinase C site. J Neurosci 17(10), 3515-3524. doi: 10.1523/jneurosci.17-10-03515.1997.
Holahan, M.R. (2015). GAP-43 in synaptic plasticity: molecular perspectives. Research and Reports in Biochemistry 5, 137-146. doi: 10.2147/Rrbc.S73846.
Holahan, M.R. (2017). A Shift from a Pivotal to Supporting Role for the Growth-Associated Protein (GAP-43) in the Coordination of Axonal Structural and Functional Plasticity. Front Cell Neurosci 11, 266. doi: 10.3389/fncel.2017.00266.
Hou, X.E., Lundmark, K., and Dahlstrom, A.B. (1998). Cellular reactions to axotomy in rat superior cervical ganglia includes apoptotic cell death. Journal of Neurocytology 27(6), 441-451. doi: Doi 10.1023/A:1006988528655.
Irie, T., Yamakawa, K., Hamon, D., Nakamura, K., Shivkumar, K., and Vaseghi, M. (2017). Cardiac sympathetic innervation via middle cervical and stellate ganglia and antiarrhythmic mechanism of bilateral stellectomy. Am J Physiol Heart Circ Physiol 312(3), H392-h405. doi: 10.1152/ajpheart.00644.2016.
Isbister, J., and Semsarian, C. (2019). Sudden cardiac death: an update. Internal Medicine Journal 49(7), 826-833. doi: 10.1111/imj.14359.
Kawashima, T. (2005). The autonomic nervous system of the human heart with special reference to its origin, course, and peripheral distribution. Anatomy and Embryology 209(6), 425-438. doi: 10.1007/s00429-005-0462-1.
Kimura, K., Ieda, M., and Fukuda, K. (2012). Development, Maturation, and Transdifferentiation of Cardiac Sympathetic Nerves. Circulation Research 110(2), 325-336. doi: doi:10.1161/CIRCRESAHA.111.257253.
Kimura, K., Ieda, M., Kanazawa, H., Yagi, T., Tsunoda, M., Ninomiya, S.-i., et al. (2007). Cardiac Sympathetic Rejuvenation. Circulation Research 100(12), 1755-1764. doi: doi:10.1161/01.RES.0000269828.62250.ab.
Kobayashi, K., and Nagatsu, T. (2012). "Chapter 7 - Tyrosine Hydroxylase," in Primer on the Autonomic Nervous System (Third Edition), eds. D. Robertson, I. Biaggioni, G. Burnstock, P.A. Low & J.F.R. Paton. (San Diego: Academic Press), 45-47.
Korshunova, I., and Mosevitsky, M. (2010). Role of the growth-associated protein GAP-43 in NCAM-mediated neurite outgrowth. Adv Exp Med Biol 663, 169-182. doi: 10.1007/978-1-4419-1170-4_11.
Kuruvilla, R., Zweifel, L.S., Glebova, N.O., Lonze, B.E., Valdez, G., Ye, H., et al. (2004). A neurotrophin signaling cascade coordinates sympathetic neuron development through differential control of TrkA trafficking and retrograde signaling. Cell 118(2), 243-255. doi: 10.1016/j.cell.2004.06.021.
Kusik, B.W., Hammond, D.R., and Udvadia, A.J. (2010). Transcriptional regulatory regions of gap43 needed in developing and regenerating retinal ganglion cells. Developmental dynamics : an official publication of the American Association of Anatomists 239(2), 482-495. doi: 10.1002/dvdy.22190.
Li, C.Y., and Li, Y.G. (2015). Cardiac Sympathetic Nerve Sprouting and Susceptibility to Ventricular Arrhythmias after Myocardial Infarction. Cardiol Res Pract 2015, 698368. doi: 10.1155/2015/698368.
Li, Z., Wang, M., Zhang, Y., Zheng, S., Wang, X., and Hou, Y. (2015). The Effect of the Left Stellate Ganglion on Sympathetic Neural Remodeling of the Left Atrium in Rats Following Myocardial Infarction. Pacing and Clinical Electrophysiology 38(1), 107-114. doi: 10.1111/pace.12513.
Lopez-Barneo, J., Ortega-Saenz, P., Pardal, R., Pascual, A., and Piruat, J.I. (2008). Carotid body oxygen sensing. Eur Respir J 32(5), 1386-1398. doi: 10.1183/09031936.00056408.

Matsuo, A., Bellier, J.P., Nishimura, M., Yasuhara, O., Saito, N., and Kimura, H. (2011). Nuclear choline acetyltransferase activates transcription of a high-affinity choline transporter. J Biol Chem 286(7), 5836-5845. doi: 10.1074/jbc.M110.147611.
Nakamura, K., Ajijola, O.A., Aliotta, E., Armour, J.A., Ardell, J.L., and Shivkumar, K. (2016). Pathological effects of chronic myocardial infarction on peripheral neurons mediating cardiac neurotransmission. Auton Neurosci 197, 34-40. doi: 10.1016/j.autneu.2016.05.001.
Nguyen, B.L., Li, H., Fishbein, M.C., Lin, S.F., Gaudio, C., Chen, P.S., et al. (2012). Acute myocardial infarction induces bilateral stellate ganglia neural remodeling in rabbits. Cardiovasc Pathol 21(3), 143-148. doi: 10.1016/j.carpath.2011.08.001.
Nguyen, L., He, Q., and Meiri, K.F. (2009). Regulation of GAP-43 at serine 41 acts as a switch to modulate both intrinsic and extrinsic behaviors of growing neurons, via altered membrane distribution. Mol Cell Neurosci 41(1), 62-73. doi: 10.1016/j.mcn.2009.01.011.
O'Keeffe, G.W., Gutierrez, H., Howard, L., Laurie, C.W., Osorio, C., Gavaldà, N., et al. (2016). Region-specific role of growth differentiation factor-5 in the establishment of sympathetic innervation. Neural Development 11(1), 4. doi: 10.1186/s13064-016-0060-3.
Olivas, A., Gardner, R.T., Wang, L., Ripplinger, C.M., Woodward, W.R., and Habecker, B.A. (2016). Myocardial Infarction Causes Transient Cholinergic Transdifferentiation of Cardiac Sympathetic Nerves via gp130. J Neurosci 36(2), 479-488. doi: 10.1523/jneurosci.3556-15.2016.
Ortega-Saenz, P., and Lopez-Barneo, J. (2020). Physiology of the Carotid Body: From Molecules to Disease. Annu Rev Physiol 82, 127-149. doi: 10.1146/annurev-physiol-020518-114427.
Pather, N., Partab, P., Singh, B., and Satyapal, K.S. (2003). The sympathetic contributions to the cardiac plexus. Surgical and Radiologic Anatomy 25(3), 210-215. doi: 10.1007/s00276-003-0113-2.
Pulgar-Sepúlveda, R., Varas, R., Iturriaga, R., Del Rio, R., and Ortiz, F.C. (2018). Carotid Body Type-I Cells Under Chronic Sustained Hypoxia: Focus on Metabolism and Membrane Excitability. Frontiers in Physiology 9(1282). doi: 10.3389/fphys.2018.01282.
Rocha, I., Rosário, L.B., de Oliveira, E.I., Barros, M.A., and Silva-Carvallho, L. (2003). Enhancement of carotid chemoreceptor reflex and cardiac chemosensitive reflex in the acute phase of myocardial infarction of the anesthetized rabbit. Basic Res Cardiol 98(3), 175-180. doi: 10.1007/s00395-003-0407-x.
Skene, J.H. (1989). Axonal growth-associated proteins. Annu Rev Neurosci 12, 127-156. doi: 10.1146/annurev.ne.12.030189.001015.
Stocco, E., Barbon, S., Tortorella, C., Macchi, V., De Caro, R., and Porzionato, A. (2020). Growth Factors in the Carotid Body-An Update. Int J Mol Sci 21(19). doi: 10.3390/ijms21197267.
Winick-Ng, W., and Rylett, R.J. (2018). Into the Fourth Dimension: Dysregulation of Genome Architecture in Aging and Alzheimer's Disease. Front Mol Neurosci 11, 60. doi: 10.3389/fnmol.2018.00060.
Wink, J., van Delft, R., Notenboom, R.G.E., Wouters, P.F., DeRuiter, M.C., Plevier, J.W.M., et al. (2020). Human adult cardiac autonomic innervation: Controversies in anatomical knowledge and relevance for cardiac neuromodulation. Auton Neurosci 227, 102674. doi: 10.1016/j.autneu.2020.102674.
Wit, A.L. (2017). Basic Electrophysiologic Mechanisms of Sudden Cardiac Death Caused by Acute Myocardial Ischemia and Infarction. Card Electrophysiol Clin 9(4), 525-536. doi: 10.1016/j.ccep.2017.07.004.
World Health Organization (2017). Cardiovascular diseases (CVDs) [Online]. World Health Organization. Available: https://www.who.int/news-room/fact-sheets/detail/cardiovascular-diseases-(cvds) [Accessed 17 May 2017].
Yokoyama, T., Lee, J.K., Miwa, K., Opthof, T., Tomoyama, S., Nakanishi, H., et al. (2017). Quantification of sympathetic hyperinnervation and denervation after myocardial infarction by three-dimensional assessment of the cardiac sympathetic network in cleared transparent murine hearts. PLoS One 12(7), e0182072. doi: 10.1371/journal.pone.0182072.

Zhou, S., Chen, L.S., Miyauchi, Y., Miyauchi, M., Kar, S., Kangavari, S., et al. (2004). Mechanisms of Cardiac Nerve Sprouting After Myocardial Infarction in Dogs. Circulation Research 95(1), 76-83. doi: doi:10.1161/01.RES.0000133678.22968.e3.
Ziegler, K.A., Ahles, A., Wille, T., Kerler, J., Ramanujam, D., and Engelhardt, S. (2018). Local sympathetic denervation attenuates myocardial inflammation and improves cardiac function after myocardial infarction in mice. Cardiovasc Res 114(2), 291-299. doi: 10.1093/cvr/cvx227.
Zipes, D.P., and Rubart, M. (2006). Neural modulation of cardiac arrhythmias and sudden cardiac death. Heart Rhythm 3(1), 108-113. doi: 10.1016/j.hrthm.2005.09.021.

SUPPLEMENTAL FIGURES

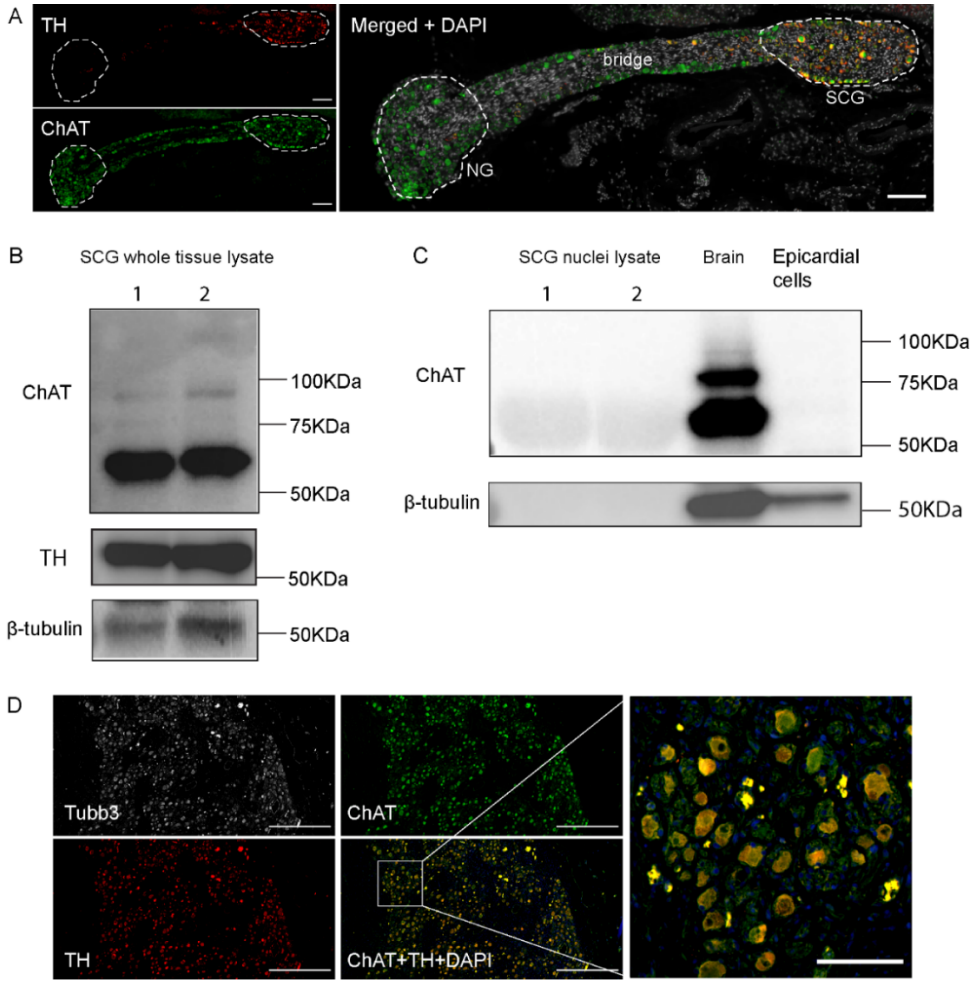

Supplemental Figure. 1 ChAT expression in murine nodose ganglion and human stellate ganglion. A. Immunofluorescence staining of TH (red) and ChAT (green) in murine NG, SCG, and the bridge between the ganglia. NG and SCG are indicated by dashed lines. Scale bar = 100 µm. B. Immunoblot analysis of ChAT or β-tubulin (loading control) in protein lysates of 4 control murine SCG displayed the expression of ChAT isoforms in SCG. C. Immunoblot analysis of ChAT and β-tubulin (loading control) in nuclei protein lysates of 4 SCG, total cell protein lysates of murine brain (positive control), and total cell protein lysates of human epicardial cells (negative control). No detection of β-tubulin in SCG nuclei lysate is aimed to confirm no cytoplasm contamination. D. Immunofluorescence staining of Tubb3 (gray) TH (red), ChAT (green) and nuclei (blue) in human stellate ganglion, enlarged image of merged channels is shown in the rightest panel. Scale bar = 500 µm. Scale bar in enlarged image = 100 µm.

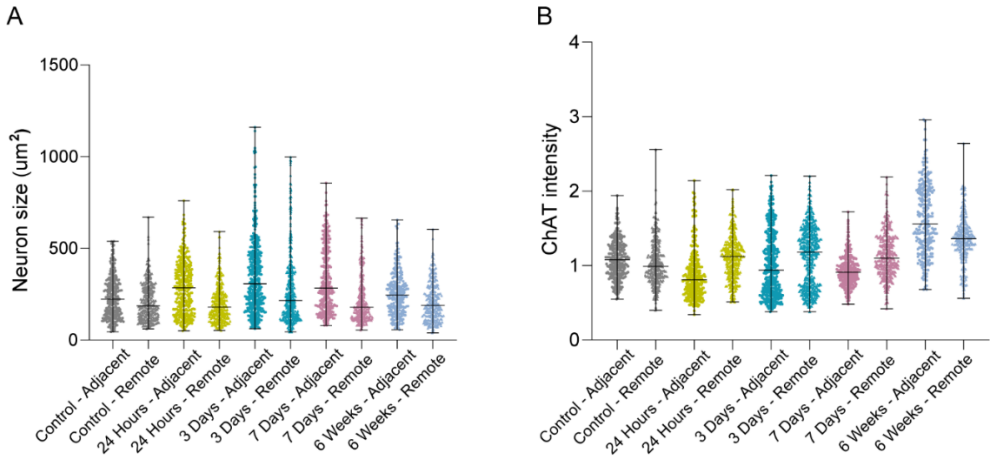

Supplemental Figure 2. Graphs related to figure. 2. A. A. cell size overview of neurons adjacent or remote to CB in control SCG and post-MI SCG at different timepoints. Each dot represents a neuronal cell. Lines indicate the medium ± range of each dataset. B. A relative ChAT intensity overview of neurons adjacent or remote to CB in control SCG and post-MI SCG at different timepoints. Each dot represents a neuronal cell. Lines indicate the medium ± range of each dataset. Relative ChAT intensity was calculated as a fold change of fluorescence intensity of neuronal ChAT to the intensity of cholinergic nerves in each corresponding ganglion (internal reference).

SUPPLEMENTAL METHODS

Immunofluorescence staining of murine nodose ganglion and human stellate ganglion

A nodose ganglion was isolated from one of 6-week post-MI mice. A human stellate ganglion was obtained as redundant material from a stellate ganglion ablation surgery. All experiments were performed according to the guidelines of the Leiden University Medical Centre (Leiden, The Netherlands). The 5 µm-thick paraffin sections were deparaffinized, pre-treated with Tris-EDTA buffer (pH 9) at 98°C for 12 min for antigen retrieval, and incubated with anti-tyrosine hydroxylase (TH)(Fisher Scientific PA14679; 1:1000), anti-choline acetyl transferase (ChAT)(Abcam ab181023; 1:1000), and anti-β-tubulin III (Tubb3)(Santa Cruz; SC-80005; 1:1000) overnight at 4°C. On the second day, the sections were incubated with secondary antibodies donkey anti-rabbit Alexa Fluor 488 (Invitrogen A-21206; 1:250), donkey anti-sheep Alexa Fluor

568 (Invitrogen A21099; 1:250) and donkey anti-mouse Alexa Fluor 647 (Invitrogen A31571; 1:250) for 1 hour, and followed by a 10 min nuclear staining with DAPI (Invitrogen D3571: 1:1000) when indicated. The slides were mounted with ProLong Gold Antifade Mountant (Invitrogen P36930) and images were captured with the Zeiss AxioscanZ1.

Western Blotting

Protein of whole ganglia tissue lysate was extracted with RIPA lysis and extraction buffer (89900; ThermoFisher) supplemented with Protease inhibitor cocktail (87785; ThermoFisher). To extract protein from nuclear fraction of the ganglia, ganglionic cells were first dissociated by 30-minute incubation in 2.5% trypsin (25200056; Thermo Fisher Scientific) followed by 30-minute incubation in 5 mg/ml collagenase type II (LS004176; Worthington) at 37°C. After centrifuge the cell suspension at 300 rcf for 10 minutes, 100 µl nuclei lysis buffer (10 mM Tris-HCl, 10 mM NaCl, 3 mM MgCl2, and 0.1%Nonidet™ P40 Substitute, 40 U/ml RNAse in Nuclease-Free Water) was added into the cell pellet, cells were mixed well in nuclei lysis buffer and incubated on ice for 8 minutes. Centrifuge the nuclei suspension at 300 rcf for 5 minutes and wash twice with nuclei wash (1X PBS with 2.0% BSA). Nuclear protein was extracted with RIPA supplemented with Protease inhibitor.

20 µg of each protein was loaded in 8 % SDS-PAGE gel for electrophoresis. Following electrophoretic separation, the proteins were transferred to a polyvinylidene difluoride membrane by wet electroblotting. Afterwards, the membrane was incubated with 5% BSA in PBS-0.1% Tween 20 (PBST) for 1 hour at RT for blocking and probed with rabbit-anti-ChAT (Abcam ab181023; 1:2000) or sheep-anti-TH (Fisher Scientific PA14679; 1:2000) primary antibodies overnight at 4°C, followed by a 1-hour incubation with HRP~Donkey-anti-Rabbit IgG(H&L) (cell signalling #7074; 1:10,000) or HRP~Donkey-anti-goat IgG(H&L)(Jackson Immuno research 705035003; 1:10,000). The target protein was visualized with a WesternBright kit (Isogen life science). After stripping, the membrane was blocked for 1 hours and incubated with rabbit-anti-βtubulin followed by our incubation with HRP-linked antibody as a protein loading reference. Images were captured by C500 western blot imaging system (Azure biosystems).